CaSCADE: Compressed Carrier and DOA Estimation

Shahar Stein Ioushua, *Student Member, IEEE*, Or Yair, *Student Member, IEEE*, Deborah Cohen, *Student Member, IEEE*, and Yonina C. Eldar, *Fellow, IEEE*

***Abstract*—Spectrum sensing and direction of arrival (DOA) estimation have both been thoroughly investigated. Estimating the support of a set of signals and their DOAs is crucial to many signal processing applications, such as cognitive radio (CR). A challenging scenario, faced by CRs, is that of multiband signals, composed of several narrowband transmissions spread over a wide spectrum each with unknown carrier frequency and DOA. The Nyquist rate of such signals is high and constitutes a bottleneck for both analog and digital processing. To alleviate the sampling rate issue, several sub-Nyquist sampling methods, such as multicoset or the modulated wideband converter (MWC), have been proposed in the context of spectrum sensing. In this paper, we first suggest an alternative sub-Nyquist sampling and signal reconstruction method to the MWC, based on a uniform linear array (ULA). We then extend our approach to joint spectrum sensing and DOA estimation and propose the CompreSsed CArrier and DOA Estimation (CaSCADE) system, composed of an L-shaped array with two ULAs. In both cases, we derive conditions for perfect recovery of the signal parameters and the signal itself and provide two reconstruction algorithms. The first is based on the ESPRIT method and the second on compressed sensing techniques. Both our joint carriers and DOA recovery algorithms overcome the well-known pairing issue between the two parameters. Simulations demonstrate joint carrier and DOA recovery from CaSCADE sub-Nyquist samples. In addition, we show that our alternative spectrum sensing system outperforms the MWC in terms of recovery error and design complexity.**

***Index Terms*—Sensor arrays, Compressed sensing, Direction-of-arrival estimation, Cognitive radio, Sampling methods.**

I. Introduction

BOTH traditional tasks of spectrum sensing and direction of arrival (DOA) estimation have been thoroughly investigated in the literature. For the first, several sensing schemes have been proposed, such as energy detection [1], matched filter [2] and cyclostationary detection [3], assuming known or identical DOAs. Well known techniques for DOA estimation include MUSIC [4], [5] and ESPRIT [6], followed by more computationally efficient algorithms such as [7], [8]. Here, the signal frequency support is typically known. However, many signal processing applications may require or at least benefit from the two combined, namely joint spectrum sensing and DOA estimation.

Cognitive Radio (CR) [9] is one such application, which aims at solving the spectrum scarcity issue by exploiting its sparsity. Spectral resources, traditionally allocated to licensed or primary users (PUs) by governmental organizations, are becoming critically scant but at the same time have been shown to be underutilized [10], [11]. These observations led to the idea of CR, which allows secondary users to opportunistically access licensed frequency bands left vacant by their primary owners, increasing spectral efficiency [9], [12]. Spectrum sensing is an essential task for CRs [13], [14], which need to constantly monitor the spectrum and detect the PUs' activity, reliably and fast [15], [16]. DOA recovery can enhance CR performance by allowing exploitation of vacant bands in space in addition to the frequency domain.

The 2D-DOA problem, which requires finding two unknown angles for each transmission and pairing them, is considered in [17], [18]. The authors suggest a modification to the traditional ESPRIT [6], which is used to estimate a single angle. However, this approach only allows the recovery of two angles and solves a separable problem. This cannot be directly extended to joint angle and frequency estimation, which is not separable. Joint DOA and carrier frequency estimation has been considered in [19], [20], where the authors developed a joint angle-frequency estimation (JAFE) algorithm. JAFE is based on an extension of ESPRIT which allows for multiple parameters to be recovered. However, this method requires additional joint diagonalization of two matrices using iterative algorithms to pair between the carrier frequencies and the DOAs of the different transmissions. In [21], the authors consider multiple interleaved sampling channels, with a fixed delay between consecutive channels. They propose a two-stage reconstruction method, where first the frequencies are recovered and then the DOAs are computed from the corresponding estimated carriers. The works described above all assume that the signal is sampled at least at its Nyquist rate, and do not consider signal reconstruction.

Many modern applications deal with wideband signals leading to high Nyquist rates. For instance, to increase the chance of finding unoccupied spectral bands, CRs have to sense a wide spectrum, leading to prohibitively high Nyquist rates. Moreover, such high sampling rates generate a large number of samples to process, affecting speed and power consumption. To overcome the rate bottleneck, several sampling methods have recently

Manuscript received August 30, 2016; revised January 8, 2017; accepted January 14, 2017. Date of publication February 6, 2017; date of current version March 14, 2017. The associate editor coordinating the review of this manuscript and approving it for publication was Dr. Yongming Huang. This work was supported in part by the European Union's Horizon 2020 research and innovation program under Grant 646804-ERC-COG-BNYQ, and in part by the Israel Science Foundation under Grant 335/14. The work of D. Cohen was supported by the Azrieli Foundation.

The authors are with the Electrical Engineering department, Technion—Israel Institute of Technology, Haifa 32000, Israel (e-mail: shahar-stein@campus.technion.ac.il; oryair@tx.technion.ac.il; deborah.co88@gmail.com; yonina@ee.technion.ac.il).

Color versions of one or more of the figures in this paper are available online at http://ieeexplore.ieee.org.

Digital Object Identifier 10.1109/TSP.2017.2664054

been proposed [14], [22], [23] that reduce the sampling rate in multiband settings below Nyquist.

The multicoset or interleaved approach adopted in [22] suffers from practical issues, as described in [23]. Specifically, the signal bandwidth can exceed the analog bandwidth of the low rate analog-to-digital converter (ADC) by orders of magnitude. Another practical issue stems from the time shift elements since it can be difficult to maintain accurate time delays between the ADCs at such high rates. The modulated wideband converter (MWC) [23], an analog front-end composed of several channels, was designed to overcome these issues. In each channel, the analog wideband signal is mixed by a periodic function, low-pass filtered and sampled at a low rate. The MWC solves carrier estimation and spectrum sensing from sub-Nyquist samples, but does not address DOA recovery.

A few works have recently considered joint DOA and spectrum sensing of multiband signals from sub-Nyquist samples. In [24], the authors consider both time and spatial compression by selecting receivers from a uniform linear array (ULA) and samples from the Nyquist grid using multicoset sampling. They exploit a mathematical relation between sub-Nyquist and Nyquist samples over a certain sensing time and recover the signal's power spectrum from the compressed samples. The frequency support and DOAs are then estimated by identifying peaks of the power spectrum, corresponding to each one of the uncorrelated transmissions. Since the power spectrum is computed over a finite sensing time, the frequency supports and angles are obtained on a grid defined by the number of samples. In [25], an L-shaped array with two interleaved (or multicoset) channels, with a fixed delay between the two, samples the signal below the Nyquist rate. Then, the carrier frequencies and the DOAs are recovered from the samples. However, the pairing between the two parameter is not discussed. Moreover, this delay-based approach suffers from the same drawbacks as the multicoset sampling scheme when it comes to practical implementation.

In this work, we first consider spectrum sensing of a multiband signal whose transmissions are assumed to have known or identical DOAs. For this scenario, we present an alternative sub-Nyquist sampling scheme to the MWC, based on a ULA of sensors. We then extend this approach to the case where both the carrier frequencies and DOAs of the transmissions composing the input signal are unknown. In this case, we propose the CompreSsed CArrier and DOA Estimation (CaSCADE) system, consisting of an L-shaped array, and perform joint DOA and carrier recovery from sub-Nyquist samples.

In the first scenario, we consider a ULA where each sensor implements one MWC channel. This configuration has two main advantages over the MWC. First, it allows for a simpler design of the mixing functions which can be identical in all sensors. Second, the ULA based system outperforms the MWC in low signal to noise ratio (SNR) regimes. This is due to the fact that since all MWC channels belong to the same sensor, they are all affected by the same additive sensor noise. In contrast, each channel of the ULA system has a different sensor with uncorrelated sensor noise between channels, allowing for noise averaging that increases SNR.

Using the ULA configuration, we are able to formulate sub-Nyquist spectrum sensing as the well known sum-of-exponents problem, which can be solved by various known methods. Here, we present two approaches to recover the carrier frequencies of the transmissions composing the input signal. The first is based on compressed sensing (CS) [26] algorithms and assumes that the carriers lie on a predefined grid. In the second technique, we drop the grid assumption and use ESPRIT [6] to estimate the frequencies. Once these are recovered, we show how the signal itself can be reconstructed. We demonstrate that the minimal number of sensors required for perfect reconstruction in noiseless settings is identical for both recovery approaches and that our system achieves the minimal sampling rate derived in [22].

Next, we extend our approach to joint spectrum sensing and DOA estimation from sub-Nyquist samples, using CaSCADE, which implements the modified MWC over an L-shaped array. Specifically, we consider several narrowband transmissions spread over a wide spectrum, impinging on an L-shaped ULA, each from a different direction. The array sensors are composed of an analog mixing front-end, implementing one channel of the MWC [23], as before. We suggest two approaches to jointly recover the carrier frequencies and DOAs of the transmissions. The first is based on CS techniques and allows recovery of both parameters assuming they lie on a predefined grid. The CS problem is formulated in such a way that no pairing issue arises between the carrier frequencies and their corresponding DOAs. The second approach, inspired by [17], [18], extends ESPRIT to the joint estimation of carriers and DOAs, while overcoming the pairing issue. Our 2D-ESPRIT algorithm can be applied to sub-Nyquist samples, as opposed to previous work which only considered the Nyquist regime.

Once the carriers and DOAs are recovered, the signal itself is reconstructed, similarly to the previous scenario. We provide sufficient conditions on our sampling system for perfect reconstruction of the carriers and DOAs, and of the signal itself, in noiseless settings. We compare our reconstruction algorithms to the Parallel Factor (PARAFAC) analysis method [27], previously proposed for the 2D-DOA problem [28], [29] in the Nyquist regime. The adaptation of PARAFAC to the joint spectrum sensing and carrier estimation from sub-Nyquist samples problem has been presented in the conference version of this paper [30].

This paper is organized as follows. In Section II, we formulate the signal model and spectrum sensing goal. Section III presents the ULA-based sub-Nyquist sampling and reconstruction schemes assuming known and identical DOA. The joint spectrum sensing and DOA estimation problem is considered in Section IV. We present the CaSCADE system along with its sampling scheme and reconstruction techniques. Numerical experiments for both systems are shown in Section V.

II. Spectrum Sensing Problem Formulation

A. Signal Model

Let $u(t)$ be a complex-valued continuous-time signal, bandlimited to $\mathcal{F} = \left[-f_{\text{Nyq}}/2, f_{\text{Nyq}}/2\right]$ and composed of up to M uncorrelated transmissions $s_i(t)$, $i \in \{1, 2, \ldots, M\}$. Each

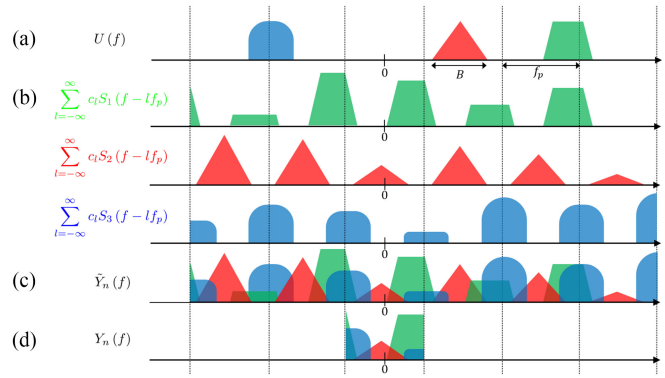

Fig. 1. The different stages of the analog mixing front-end at the nth sensor. (a) The input signal in the frequency domain $U(f)$ with $M=3$ different source signals. (b) Each replicated source signal (after mixing). (c) Replicated input signal $\tilde{Y}_n(f)$ (after mixing). (d) Baseband signal $Y_n(f)$ after LPF.

transmission $s_i(t)$ is modulated by a carrier frequency $f_i \in \mathbb{R}$, such that

$$u(t) = \sum_{i=1}^{M} s_i(t)\, e^{j2\pi f_i t}. \tag{1}$$

Assume that $s_i(t)$ are bandlimited to $\mathcal{B} = \left[-1/2T,\ 1/2T\right]$ and disjoint, namely $\min_{i\neq j}\{|f_i - f_j|\} > B$, where $B = |\mathcal{B}|$. Formally, the Fourier transform of $u(t)$, defined by

$$U(f) = \int_{-\infty}^{\infty} u(t) e^{-j2\pi f t} dt = \sum_{i=1}^{M} S_i(f - f_i), \tag{2}$$

where $S_i(f)$ is the Fourier transform of $s_i(t)$, is zero for every $f \notin \mathcal{F}$. All source signals are assumed to have identical and known angles of arrival (AOA) $\theta \neq 90°$. A typical source signal $u(t)$ is depicted in the frequency domain in Fig. 1(a). The corresponding signal set is defined formally in the following definition.

Definition 1: The set $\mathcal{M}_1$ contains all signals $u(t)$, such that the support of the Fourier transform $U(f)$ is contained within a union of M disjoint intervals in $\mathcal{F}$. Each of the bandwidths does not exceed B and all the transmissions composing $u(t)$ have identical and known AOA $\theta \neq 90°$.

We wish to design a sampling and reconstruction system for signals from the model $\mathcal{M}_1$ which satisfies the following properties:

1) The system has no prior knowledge on the carrier frequencies.
2) The sampling rate should be as low as possible.

Let $\mathbf{s}(t) = [s_1(t), s_2(t), \cdots, s_M(t)]^T$ be the source signals vector, $\mathbf{S}(f) = [S_1(f), S_2(f), \cdots, S_M(f)]^T$ the signal Fourier transform vector, and $\boldsymbol{f} = [f_1, f_2, \cdots, f_M]^T$ the carrier frequencies vector. Our goal is then to design a sampling and reconstruction method in order to recover $\boldsymbol{f}$ and $\mathbf{s}(t)$ from sub-Nyquist samples of $u(t)$. In the reconstruction phase, we address two separate objectives:

1) Frequency recovery, i.e. recovering only $\boldsymbol{f}$.
2) Full spectrum recovery, i.e. recovering both $\boldsymbol{f}$ and $\mathbf{s}(t)$.

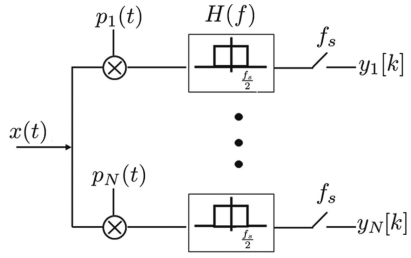

Fig. 2. MWC system.

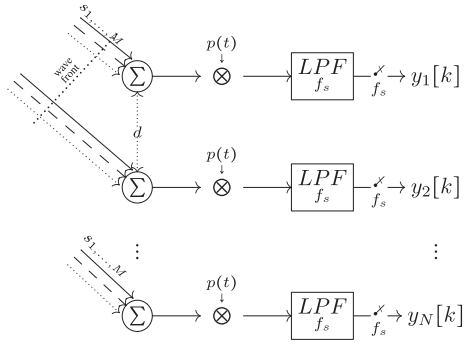

Fig. 3. ULA configuration with N sensors, with distance d between two adjacent sensors. Each sensor includes an analog front-end composed of a mixer with the same periodic function $p(t)$, a LPF and a sampler, at rate f_s.

B. Multicoset Sampling and the MWC

It was previously shown in [22], that if $MB < \frac{f_{\text{Nyq}}}{2}$, then the minimal sampling rate to allow blind reconstruction of $u(t)$ is $2MB$, namely twice the Landau rate [31]. Concrete algorithms for blind recovery achieving the minimal rate were developed in [22] based on multicoset sampling and in [23] based on the MWC. Unfortunately, the implementation of multicoset sampling is problematic due to the inherent analog bandwidth of the ADCs and the required synchronization between time shift elements [23].

The MWC achieves the minimal sampling rate and has been implemented in practice [23], [32]. This system is composed of N parallel channels. Each channel consists of an analog mixing front-end in which $u(t)$ is multiplied by a periodic mixing function $p_n(t), 1 \leq n \leq N$. This multiplication aliases the spectrum, such that each spectral band appears in baseband. We denote by T_p the period of $p_n(t)$ and require $f_p = 1/T_p \geq B$. The signal then goes through a low-pass filter (LPF) with cut-off frequency $f_s/2$ and is sampled at rate $f_s \geq f_p$. Finally, $u(t)$ is reconstructed from the low rate samples using CS techniques. An illustration of the MWC is shown in Fig. 2.

A known difficulty of the MWC is choosing appropriate periodic functions $p_n(t)$ so that their Fourier coefficients fulfill CS requirements [33]. In this work, we suggest an alternative implementation of the MWC, based on a ULA, which overcomes this difficulty, and satisfies the properties described above. In addition, our ULA based system, shown in Fig. 3, is more robust to noise, as we demonstrate via simulations. In Section IV, we show that the system can also be used for DOA recovery.

III. ULA Based MWC

A. System Description

Our sensing system consists of a ULA composed of N sensors, with two adjacent sensors separated by a distance d, such that $d < \frac{c}{|\cos(\theta)|f_{\text{Nyq}}}$, where c is the speed of light. All sensors have the same sampling pattern implementing a single channel of the MWC; the received signal is multiplied by a periodic function $p(t)$ with period $T_p = 1/f_p$, low-pass filtered with a filter that has cut-off frequency $f_s/2$ and sampled at the low rate f_s. The system is illustrated in Fig. 3. The only requirement on $p(t)$ is that none of its Fourier series coefficients within the signal's Nyquist bandwidth are zero.

In the next section, we show how we can recover both the carrier frequencies $\boldsymbol{f}$ and $\mathbf{s}(t)$, which uniquely determine the signal $u(t)$, from the samples at the output of Fig. 3. We demonstrate that the minimal number of sensors required by both our reconstruction methods is $N = 2M$, with each sensor sampling at the minimal rate of $f_s = B$ to allow for perfect signal recovery. This leads to a minimal sampling rate of $2MB$, as shown in [22], which is assumed to be less than f_{Nyq}. With high probability, the minimal number of sensors reduces to $M + 1$.

In the remainder of this section, we describe our ULA based sampling scheme and derive conditions for perfect recovery of the carrier frequencies $\boldsymbol{f}$ and the transmissions $\mathbf{s}(t)$. We then provide concrete recovery algorithms.

B. Frequency Domain Analysis

We start by deriving the relation between the sample sequences from the nth sensor and the unknown transmissions $s_i(t)$ and corresponding carrier frequencies $\boldsymbol{f}$. To this end, we introduce the following definitions

$$\mathcal{F}_p \triangleq \left[-f_p/2,\ \ f_p/2\right], \quad \mathcal{F}_s \triangleq \left[-f_s/2,\ \ f_s/2\right]. \tag{3}$$

Consider the received signal $u_n(t)$ at the nth sensor of the ULA

$$u_n(t) = \sum_{i=1}^{M} s_i(t+\tau_n)e^{j2\pi f_i(t+\tau_n)} \approx \sum_{i=1}^{M} s_i(t)e^{j2\pi f_i(t+\tau_n)}, \tag{4}$$

where

$$\tau_n = \frac{dn}{c}\cos(\theta) \tag{5}$$

is the accumulated phase at the nth sensor with respect to the first sensor. The approximation in (4) stems from the narrowband assumption on the transmissions $s_i(t)$. The Fourier transform of the received signal $u_n(t)$ is then given by

$$U_n(f) = \sum_{i=1}^{M} S_i(f - f_i)\, e^{j2\pi f_i \tau_n}. \tag{6}$$

In each sensor, the received signal is first mixed with the periodic function $p(t)$ prior to filtering and sampling. Since $p(t)$ is periodic with period $T_p = 1/f_p$, it can be represented by its Fourier series

$$p(t) = \sum_{l=-\infty}^{\infty} c_l e^{j2\pi l f_p t}, \tag{7}$$

where

$$c_l = \frac{1}{T_p}\int_0^{T_p} p(t)e^{-j2\pi l f_p t}\mathrm{d}t. \tag{8}$$

The Fourier transform of the analog multiplication $\tilde{y}_n(t) = u_n(t)p(t)$ is evaluated as

$$\begin{aligned}\tilde{Y}_n(f) &= \int_{-\infty}^{\infty} u_n(t)\, p(t)\, e^{-j2\pi f t}\mathrm{d}t \\ &= \sum_{l=-\infty}^{\infty} c_l U_n(f - l f_p).\end{aligned} \tag{9}$$

The mixed signal $\tilde{Y}_n(f)$ is thus a linear combination of f_p- shifted and c_l- scaled copies of $U_n(f)$. Since $U(f) = 0$, $\forall f \notin \mathcal{F}$, the sum in (9) contains at most $\left\lceil \frac{f_{\text{Nyq}}}{f_p} \right\rceil$ nonzero terms, for each f. Figs. 1(b)–(c) depict each transmission and the resulting signal after mixing, respectively.

Substituting (6) into (9), we have

$$\tilde{Y}_n(f) = \sum_{l=-\infty}^{\infty} c_l \sum_{i=1}^{M} S_i(f - f_i - l f_p)\, e^{j2\pi f_i \tau_n}.$$

Denote by $h(t)$ and $H(f)$ the impulse and frequency responses of an ideal LPF with cut-off frequency f_s, respectively. After filtering $\tilde{y}_n(t)$ with $h(t)$, we have

$$\begin{aligned}Y_n(f) &= \tilde{Y}_n(f)\, H(f) \\ &= \begin{cases} \sum_{l=-\infty}^{\infty} c_l \sum_{i=1}^{M} S_i(f - f_i - l f_p)\, e^{j2\pi f_i \tau_n}, & f \in \mathcal{F}_s \\ 0, & f \notin \mathcal{F}_s. \end{cases}\end{aligned}$$

Note that $Y_n(f)$ only contains frequencies in the interval $\mathcal{F}_s$, due to the lowpass operation. Therefore, it is composed of a finite number of aliases of $U_n(f)$. Consequently, we can write

$$\begin{aligned}Y_n(f) &= \sum_{l=-L_0}^{L_0} c_l \sum_{i=1}^{M} S_i(f - f_i - l f_p)\, e^{j2\pi f_i \tau_n} \\ &= \sum_{i=1}^{M} e^{j2\pi f_i \tau_n} \sum_{l=-L_0}^{L_0} c_l S_i(f - f_i - l f_p) \\ &= \sum_{i=1}^{M} \tilde{S}_i(f)\, e^{j2\pi f_i \tau_n},\end{aligned}$$

where L_0 is the smallest integer such that the sum contains all nonzero contributions, i.e. $L_0 = \left\lceil \frac{f_{\text{Nyq}} + f_s}{2 f_p} \right\rceil - 1$, and

$$\tilde{S}_i(f) \triangleq \sum_{l=-L_0}^{L_0} c_l S_i(f - f_i - l f_p), \quad f \in \mathcal{F}_s. \tag{10}$$

The corresponding $Y_n(f)$ after filtering is depicted in Fig. 1(d). Note that in the interval $\mathcal{F}_p$, $\tilde{S}_i(f)$ is a cyclic shifted and scaled (by known factors $\{c_l\}$) version of $S_i(f)$, as shown in Fig. 4.

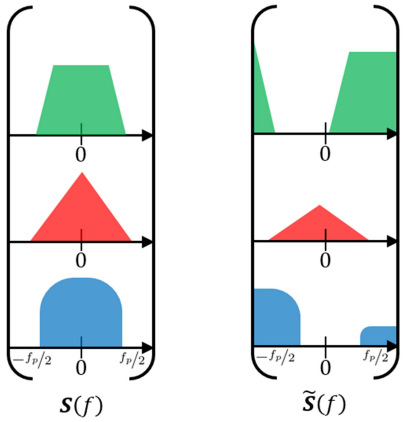

Fig. 4. The left pane shows the original source signals at baseband (before modulation). The right pane presents the output signals at baseband $\tilde{S}(f)$ after modulation, mixing and filtering.

After sampling, the discrete-time Fourier transform (DTFT) of the nth sequence $x_n[k] \triangleq y_n(kT_s)$ is expressed as

$$X_n\left(e^{j2\pi fT_s}\right) = \sum_{i=1}^{M} W_i\left(e^{j2\pi fT_s}\right) e^{j2\pi f_i \tau_n}, \quad f \in \mathcal{F}_s, \quad (11)$$

where we define $w_i[k] \triangleq \tilde{s}_i(kT_s)$ and $W_i\left(e^{j2\pi fT_s}\right) = \text{DTFT}\{w_i[k]\}$. It is convenient to write (11) in matrix form as

$$\mathbf{X}(f) = \mathbf{A}\mathbf{W}(f), \quad f \in \mathcal{F}_s. \quad (12)$$

Here, $\mathbf{X}(f)$ is of length N with nth element $X_n(f) = X_n\left(e^{j2\pi fT_s}\right)$, the unknown vector $\mathbf{W}(f)$ is of length M, with its ith entry $W_i(f) = W_i\left(e^{j2\pi fT_s}\right)$ and the matrix $\mathbf{A}$ depends on the unknown carrier frequencies vector $\boldsymbol{f}$, and is defined by

$$\mathbf{A} = \begin{pmatrix} e^{j2\pi f_1\tau_1} & \dots & e^{j2\pi f_M\tau_1} \\ \vdots & & \vdots \\ e^{j2\pi f_1\tau_N} & \dots & e^{j2\pi f_M\tau_N} \end{pmatrix}. \quad (13)$$

In the time domain, we have,

$$\mathbf{x}[k] = \mathbf{A}\mathbf{w}[k], \quad k \in \mathbb{Z}, \quad (14)$$

where $\mathbf{x}[k]$ has nth element $x_n[k]$ and $\mathbf{w}[k]$ is a vector of length M with ith element $w_i[k]$.

In the next section, we derive sufficient conditions for (14) to have a unique solution, namely for perfect recovery of the carrier frequencies $\boldsymbol{f}$ and the transmissions $\mathbf{s}(t)$ from the low rate samples $\mathbf{x}[k]$.

C. Choice of Parameters

In order to enable perfect blind reconstruction of both the carrier frequencies $\boldsymbol{f}$ and transmissions $\mathbf{s}(t)$ in noiseless settings, we first require (14) to have a unique solution. In addition, we need to ensure that $\mathbf{s}(t)$ can be uniquely recovered from $\mathbf{w}[k], k \in \mathbb{Z}$. Theorem 1 presents sufficient conditions for (14) to have a unique solution. Then, Theorem 2 specifies sufficient conditions for perfect recovery of $\mathbf{s}(t)$.

1) Carrier Frequency Recovery: We first consider sufficient conditions on the ULA to allow for perfect reconstruction of $\boldsymbol{f}$.

Theorem 1: Let $u(t)$ be an arbitrary signal in $\mathcal{M}_1$ and consider a ULA with spacing $d < \frac{c}{|\cos(\theta)|f_{\text{Nyq}}}$ and steering matrix $\mathbf{A}$. If:

- (c1) $N > 2M - \dim(\text{span}(\mathbf{w}))$
- (c2) $\dim(\text{span}(\mathbf{w})) \geq 1$,

then (14) has a unique solution $(\boldsymbol{f}, \mathbf{w})$.

Proof: From the assumption of disjoint transmissions, we have $f_i \neq f_j$, for $i \neq j$. Thus, if $d < \frac{c}{|\cos(\theta)|f_{\text{Nyq}}}$, then it holds that $d \neq \frac{ck}{|\cos(\theta)|} \cdot \frac{1}{|f_i - f_j|}$, $\forall k \in \mathbb{Z}$, $\forall i \neq j$, and $e^{j2\pi f_i\tau_n} \neq e^{j2\pi f_j\tau_n}$ for $1 \leq n \leq N-1$, with τ_n defined in (5). It follows that $\mathbf{A}$ is a Vandermonde matrix with $M \leq N$, and thus, $\text{rank}(\mathbf{A}) = M$, that is $\mathbf{A}$ is full column rank.

Since $d < \frac{c}{|\cos(\theta)|f_{\text{Nyq}}}$, we have that $2\pi f_i\tau_1 \in (-\pi, \pi]$. The proof then follows directly from Proposition 2 in [34].

Proposition 1 (Proposition 2, [34]): If $(\boldsymbol{f}, \mathbf{w})$ is a solution to (14), and

$$N > 2M - \dim(\text{span}(\mathbf{w})), \quad \dim(\text{span}(\mathbf{w})) \geq 1$$

then $(\boldsymbol{f}, \mathbf{w})$ is the unique solution of (14). ■

Note that $\dim(\text{span}(\mathbf{w})) < 1$ iff $u(t) \equiv 0$, that is the received signal does not contain any transmission.

2) Signal Recovery: While Theorem 1 guarantees the uniqueness of $(\boldsymbol{f}, \mathbf{w})$, some additional conditions need to be imposed in order to uniquely derive $\mathbf{s}(t)$ from $\mathbf{w}$, as $\mathbf{w}$ is a sampled permutation of $\mathbf{s}(t)$. Obviously, in order to be able to achieve perfect reconstruction of $\mathbf{s}(t)$, the preprocessing of the signal (i.e mixing with $p(t)$ and filtering with $h(t)$) should not cause any loss of information. The following lemma presents conditions on $p(t)$ and $H(f)$ so that each entry of the processed signal vector $\tilde{\mathbf{S}}(f)$ is a cyclic shift (up to scaling by known factors $\{c_l\}$) of the matching entry of the original source signal vector $\mathbf{S}(f)$, as shown in Fig. 4. In particular, the transformation between $\mathbf{S}(f)$ and $\tilde{\mathbf{S}}(f)$ should be invertible so that the former can be recovered from the latter.

Lemma 1: If $f_s \geq f_p \geq B$ and $c_l \neq 0$ for all $l \in \{-L_0, \dots, L_0\}$, where c_l is defined in (8), then for all $f' \in \mathcal{F}_p$, there exists a unique $k \in \mathbb{Z}$, such that

$$\tilde{S}_i(f') = c_k S_i(f' - f_i - kf_p). \quad (15)$$

Proof: Consider the ith transmission. In the interval $\mathcal{F}_p$, the output of the LPF $H(f)$, namely $\tilde{S}_i(f)$, is given by

$$\tilde{S}_i(f) = \sum_{l=-L_0}^{L_0} c_l S_i(f - f_i - lf_p), \ f \in \mathcal{F}_p. \quad (16)$$

Since $f_p \geq B$, the sum in (16) is over disjoint bands and only one of its elements is nonzero for each f. Equation (15) is true for k that satisfies $f' - f_i - kf_p \in \mathcal{F}_p$, since for any other $k' \neq k$, $f' - f_i - k'f_p \notin \mathcal{F}_p$ and $\tilde{S}_i(f' - f_i - k'f_p) = 0$. ■

If $f_s \geq f_p \geq B$, then the sampling rate obeys the Nyquist rate of $\tilde{S}_i(f)$. Together with Lemma 1 this ensures that $\mathbf{s}(t)$ can be reconstructed from the low rate samples $\mathbf{x}[k]$, as incorporated in the following theorem.

Theorem 2: Let $u(t)$ and the ULA be as in Theorem 1 and let $(\boldsymbol{f}, \mathbf{w})$ be the unique solution of (14). If:

- (c1) $c_l \neq 0$ for all $l \in \{-L_0, \ldots, L_0\}$, where c_l is defined in (8)
- (c2) $f_s \geq f_p \geq B$,

then $\{s_i(t)\}_{i=1}^{M}$ can be uniquely recovered from $\mathbf{x}[k]$.

Proof: Consider the ith transmission and let $f' \in \mathcal{B} \subseteq \mathcal{F}_p$. Since $s_i(t)$ is bandlimited to $\mathcal{B}$, it holds that

$$W_i\left(e^{j2\pi f' T_s}\right) = \tilde{S}_i(f') = c_{l_a} S_i(f' - f_i - l_a \cdot f_p), \quad (17)$$

where the last equality follows from Lemma 1. Since $c_{l_a} \neq 0$, we have

$$S_i(f' - f_i - l_a \cdot f_p) = \frac{1}{c_{l_a}} W_i\left(e^{j2\pi f' T_s}\right), \quad (18)$$

or, after a change of variables,

$$S_i(f') = \frac{1}{c_{l_a}} W_i\left(e^{j2\pi (f' + f_i + l_a \cdot f_p) T_s}\right), \quad (19)$$

where l_a is given by

$$l_a = \left\lfloor \frac{f_i + f' + f_p/2}{f_p} \right\rfloor, \quad (20)$$

completing the proof. ■

Note that l_a, defined in (20), can only be the index of one of the two f_p-bins that may overlap with the ith transmission's support.

3) Minimal Sampling Rate: It was previously proved in [22] that the minimal sampling rate for perfect blind reconstruction of a signal in the model $\mathcal{M}_1$ is $2MB$. The sampling rate in our ULA based scheme is governed by B and $\dim(\text{span}(\mathbf{w}))$, where $1 \leq \dim(\text{span}(\mathbf{w})) \leq M$. Therefore, in the worst case, the minimal sampling rate that can be achieved is $2MB$, in accordance with [22]. With high probability, $\dim(\text{span}(\mathbf{w})) = M$ and the minimal rate becomes as low as $(M+1)B$.

If our sole objective is carrier frequency recovery, then we can further reduce the sampling rate of each channel f_s below B. However, in this case, the signal $W_i\left(e^{j2\pi f T_s}\right)$ is an aliased version of $\tilde{S}_i(f)$. A possible, though unlikely, consequence of the aliasing is that for some transmission, the folded versions of $\tilde{S}_i(f)$ cancel each other and result in $W_i\left(e^{j2\pi f T_s}\right) \equiv 0$. In such a case, $W_i\left(e^{j2\pi f T_s}\right)$ and the corresponding ith column of the steering matrix will not appear in (14). Nevertheless, this unlikely scenario will not affect the recovery of the other signals carrier frequencies. Carrier recovery is possible for each $s_i(t)$ such that $W_i\left(e^{j2\pi f T_s}\right) \neq 0$ for some $f \in \mathcal{F}_s$, even if $W_i\left(e^{j2\pi f T_s}\right)$ suffers from loss of information due to folding.

D. Reconstruction Methods

To solve (14), one can use any adequate DOA algorithm to recover the carriers directly from the low rate samples. In this section, we propose two such reconstruction methods, provided as representatives of subspace and CS [26] techniques. Once the carriers are estimated, the transmissions $\mathbf{s}(t)$ may be found by inverting (14) and using the relation in (19).

Algorithm 1: ESPRIT.

Input:

- Q snapshots of the sensors measurements $\mathbf{x}[k]$

Output:

- $\hat{\boldsymbol{f}}$ - estimated carriers frequencies

Algorithm:

1) Estimate the sample covariance $\mathbf{R} = \sum_{k=1}^{Q} \mathbf{x}[k]\mathbf{x}^H[k]$
2) Decompose $\mathbf{R}$ using the singular value decomposition: $\mathbf{R} = \mathbf{U}\boldsymbol{\Sigma}\mathbf{V}^H$
3) Extract signal subspace: $\mathbf{U}_s = \left[\mathbf{u}^1, \ldots, \mathbf{u}^M\right]$, the first M left singular vectors of $\mathbf{R}$
4) Define: $\mathbf{U}_1 = \left[\mathbf{u}^1, \ldots, \mathbf{u}^{M-1}\right]$, $\mathbf{U}_2 = \left[\mathbf{u}^2, \ldots, \mathbf{u}^M\right]$
5) Perform least squares recovery:
   a) $\boldsymbol{\Psi} = \mathbf{U}_1^{\dagger}\mathbf{U}_2$
   b) $\hat{\boldsymbol{f}} = \frac{\angle(\text{eig}(\boldsymbol{\Psi}))c}{2\pi d \cos(\theta)}$

1) ESPRIT Approach: One practical method to obtain a solution $(\hat{\boldsymbol{f}}, \hat{\mathbf{w}})$ is by using the ESPRIT algorithm [6] on the measurement set $\mathbf{x}[k]$, as in [34] (Section C.). We can either assume that the number of source signals M is known or first estimate it using the minimum description length (MDL) algorithm [6], for example.

One of the conditions needed to use ESPRIT is that the correlation matrix $\mathbf{R}_w = \sum_{k\in\mathbb{Z}} \mathbf{w}[k]\mathbf{w}^H[k]$ is positive definite. From [34] (Proposition 3), if $\dim(\text{span}(\mathbf{w})) = M$, then $\mathbf{R}_w \succ 0$. Therefore, the authors in [34] distinguish between two cases. The first, where $\mathbf{R}_w \succ 0$, is referred to as the uncorrelated case. Here, ESPRIT is directly applied on $\mathbf{R} = \sum_{k=1}^{Q} \mathbf{x}[k]\mathbf{x}^H[k]$, with Q is the number of snapshots. The main steps of ESPRIT are summarized in Algorithm 1. In the algorithm description, $\angle(\cdot)$ denotes the phase of its argument and $\text{eig}(\boldsymbol{\Psi})$ is a vector of the eigenvalues of $\boldsymbol{\Psi}$.

If $\dim(\text{span}(\mathbf{w})) < M$, then the rank of the correlation matrix $\mathbf{R}$ is less than M. In this case, an additional step is implemented to construct a smoothed correlation matrix of rank M, before applying ESPRIT. This scenario is referred to as the correlated case [34]. The smoothed correlation matrix is given by

$$\bar{\mathbf{R}} = \frac{1}{V} \sum_{l=1}^{V} \sum_{k=1}^{Q} \mathbf{x}_l[k]\, \mathbf{x}_l^H[k], \quad (21)$$

where $V \triangleq N - M$ and

$$\mathbf{x}_l[k] \triangleq [x_l[k], x_{l+1}[k], \cdots, x_{l+M}[k]]^T, \quad 1 \leq l \leq V. \quad (22)$$

Note that in order to be able to construct the smoothed correlation matrix, we require $N > 2M - \dim(\text{span}(\mathbf{w}))$, which is exactly condition (c2) in Theorem 1.

Once the carrier frequencies f_i are recovered, the steering matrix $\mathbf{A}$, defined in (13) is constructed. The vector $\mathbf{W}(f)$ is then obtained by inverting the steering matrix,

$$\mathbf{W}(f) = \mathbf{A}^{\dagger}\mathbf{X}(f), \quad (23)$$

and the source signal vector is computed using (19).

2) CS Approach: Suppose that the carrier frequencies f_i lie on a grid $\{\delta l\}_{l=-L}^{L}$, with $L = \frac{f_{\text{Nyq}}}{2\delta}$. Here, δ is a parameter of the recovery algorithm that defines the grid resolution. Equation (14) then becomes

$$\mathbf{x}[k] = \mathbf{G}\mathbf{w}[k], \quad k \in \mathbb{Z}, \tag{24}$$

where $\mathbf{G}$ is a $N \times (2L+1)$ matrix with (n,l) element $G_{nl} = e^{j2\pi\tau_n l\delta}$. The nonzero elements of the sparse $(2L+1)\times 1$ vector $\mathbf{w}[k]$ have unknown indices $l_i = \frac{f_i}{\delta}$ for $1 \le i \le M$.

The set of equations (24) represents an infinite number of linear systems with joint sparsity. Such systems are known as infinite measurement vectors (IMV) in the CS literature [35]. We use the support recovery paradigm from [22] that produces a finite system of equations, called multiple measurement vectors (MMV) from an infinite number of linear systems. This reduction is performed by what is referred to as the continuous to finite (CTF) block [26], [35].

From (24), we have

$$\mathbf{R} = \mathbf{G}\mathbf{R}_w^g\mathbf{G}^H \tag{25}$$

where $\mathbf{R} = \sum_{k\in\mathbb{Z}} \mathbf{x}[k]\mathbf{x}^H[k]$ is an $N \times N$ matrix and $\mathbf{R}_w^g = \sum_{k\in\mathbb{Z}} \mathbf{w}[k]\mathbf{w}^H[k]$ is an $M \times M$ matrix. We then construct a frame $\mathbf{V}$ such that $\mathbf{R} = \mathbf{V}\mathbf{V}^H$. Clearly, there are many possible ways to select $\mathbf{V}$. We construct it by performing an eigendecomposition of $\mathbf{R}$ and choosing $\mathbf{V}$ as the matrix of eigenvectors corresponding to the nonzero eigenvalues. We then define the following linear system

$$\mathbf{V} = \mathbf{G}\mathbf{U}. \tag{26}$$

From [22] (Propositions 2-3), the support of the unique sparsest solution of (26) is the same as the support of the original set of equations (24). Equation (26) can be solved using any MMV CS algorithm, such as simultaneous orthogonal matching pursuit (SOMP) [26].

Once the support S of $\mathbf{U}$, namely the support of $\mathbf{W}(f)$, is recovered, the carrier frequencies f_i are computed using $f_i = l_i\delta$, with $l_i \in S$, and the steering matrix $\mathbf{A}$, defined in (13) is constructed. The vectors $\mathbf{w}[k]$ and $\mathbf{s}(t)$ are then obtained using (23) and (19), respectively.

Theorem 3 shows that the conditions for perfect recovery of $\mathbf{w}[k]$ from (24) are identical to those derived in the previous section.

Theorem 3: Let $u(t)$ be an arbitrary signal within $\mathcal{M}_1$ and consider a ULA with spacing $d < \frac{c}{|\cos(\theta)|f_{\text{Nyq}}}$. The minimal number of sensors required for perfect recovery of $\mathbf{w}[k]$ in (24) in a noiseless environment is $N > 2M - \dim(\text{span}(\mathbf{w}))$.

Proof: If $d < \frac{c}{|\cos(\theta)|f_{\text{Nyq}}}$, then $\mathbf{G}$ is a Vandermonde matrix, and therefore has full spark, namely $\text{spark}(\mathbf{G}) = M$. From the MMV recovery condition [36], we then have

$$M < \frac{\text{spark}(\mathbf{G}) - 1 + \text{rank}(\mathbf{V})}{2}, \tag{27}$$

where $1 \le \text{rank}(\mathbf{V}) \le M$. Finally, it holds that

$$\text{rank}(\mathbf{V}) = \dim(\text{span}(\mathbf{x})) = \dim(\text{span}(\mathbf{w})), \tag{28}$$

where the last equality follows from the fact that $\mathbf{G}$ is full spark. ■

TABLE I
MAIN PROPERTIES OF THE ULA BASED AND MWC SYSTEM

	ULA based system	MWC
Periodic functions	one function for all sensors	one function per channel
Number of samplers	N - number of sensors	N - number of channels
Minimal sampling rate (average)	$(M+1)B$	$(M+1)B$
Minimal sampling rate (worst)	$2MB$	$2MB$
Practical sampling rate	Nf_s	Nf_s

In the worst case, it holds that $\text{rank}(\mathbf{V}) = \dim(\text{span}(\mathbf{w})) = 1$ and the MMV processing does not improve the recovery ability over the single measurement vector case. The required number of sensors is then $2M$, leading to a minimal sampling rate of $2MB$. With high probability, $\text{rank}(\mathbf{V}) = \dim(\text{span}(\mathbf{w})) = M$ and the number of sensors needed is reduced to $M+1$.

E. Comparison with the MWC

Both our ULA based system and the MWC [23] allow for reconstruction of multiband signals from samples obtained below the Nyquist rate. The ULA approach adopts the same sampling principle as the MWC but the two differ in several aspects. Both systems use the same amount of mixers, LPFs and samplers. However, the MWC uses one sensor composed of N analog processing channels, whereas the ULA scheme uses N sensors, each consisting of one channel. Since the MWC consists of a single sensor, all the MWC channels are affected by the same antenna noise. In the ULA system, each channel originates from a different sensor and therefore has different antenna noise, uncorrelated with the others. Another difference between the systems arises from the CS point of view. When using CS reconstruction methods an important property is the restricted isometry property (RIP) of the sensing matrix [26], [33]. In the ULA scheme the sensing matrix is a Vandermonde matrix of exponents, known to have poor RIP in general. In the MWC, we design the sensing matrix by choosing the mixing functions $\{p_n(t)\}$, and thus control its RIP. Nevertheless, choosing appropriate mixing functions can be difficult. Additionally, the CS reconstruction approach for the ULA system uses a grid for the carrier frequencies, while the MWC can retrieve carrier frequencies from the continuous spectrum using CS algorithms. As mentioned above, a known difficulty of the MWC is choosing appropriate mixing functions $\{p_n(t)\}$ so that the original signal can be reconstructed. The ULA scheme allows for all sensors to use the same function $p(t)$ and this function does not have any limitation other than $f_p > B$ and $c_l \neq 0$ for all $l \in \{-L_0, \ldots, L_0\}$ making its design an easy task. Finally, the ULA configuration can be extended to allow for joint carrier and DOA recovery, as shown in Section IV. Table I summarizes the main properties of each system.

IV. JOINT SPECTRUM SENSING AND DOA RECOVERY

We now show how our ULA based system can be expanded to allow for joint recovery of the carrier frequencies and the AOAs. This is the main advantage of our system with respect to the MWC. We present the CaSCADE system, consisting of

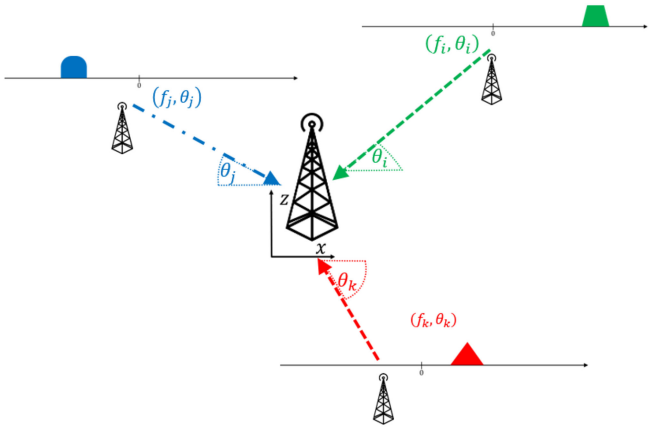

Fig. 5. Example of $M = 3$ source signals in the xz plane. Each transmission is associated with a carrier frequency f_i and AOA θ_i.

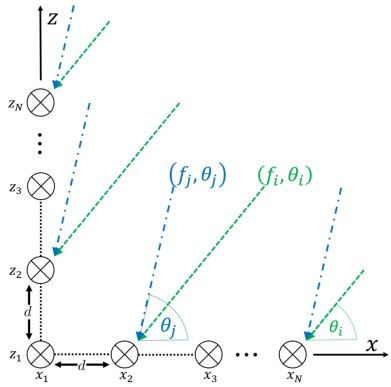

Fig. 6. CaSCADE system: L-shaped array with N sensors along the x axis and N sensors along the z axis including a common sensor at the origin.

an L-shaped array composed of two orthogonal ULAs with an identical sampling scheme.

Specifically, we consider the problem where the source signals $s_i(t), 1 \le i \le M$ have both unknown and different carrier frequencies f_i and AOAs θ_i. The main difference between this scenario and the one that has been discussed in the previous sections is the additional unknown AOAs vector $\boldsymbol{\theta} = [\theta_1, \theta_2, \cdots, \theta_M]^T$. This problem can be treated as a 2D-DOA recovery problem, where two angles are traditionally recovered. In our case, the second variable is the signal's carrier frequency instead of an additional angle. The 2D-DOA problem requires both finding the two unknown angles and pairing them. Previous work [17], [18] suggests a modification to the ESPRIT algorithm, that achieves automatic pairing between the two estimated factors, by simultaneous singular value decomposition (SVD) of two cross-correlation matrices. We further develop this approach, derived in the Nyquist regime, to perform recovery from sub-Nyquist samples.

A. Signal Model

In this scenario, for simplicity, we consider a statistical model. Let $u(t)$ and $s_i(t)$ be defined as in the previous section, with Fourier transforms $U(f)$ and $S_i(f)$, accordingly. The signals $s_i(t)$ are considered to be within the xz plane and associated with an AOA θ_i, where θ_i is measured from the positive side of the x axis. All signals are assumed to be far-field, non coherent, wide-sense stationary with zero mean and uncorrelated, i.e. for all t, $\mathbb{E}\left[s_i(t)\,\bar{s}_j(t)\right] = 0$ for $i \neq j$, with $\sigma_i^2 = \mathbb{E}\left[s_i^2(t)\right] \neq 0$. Fig. 5 illustrates our signal model. To ensure an array structure deprived of ambiguity, we assume that the electronic angles, namely $f_i \cos(\theta_i)$ and $f_i \sin(\theta_i)$, are distinct [37], [38], namely, for $i \neq j$,

$$f_i \cos(\theta_i) \neq f_j \cos(\theta_j), \;\; f_i \sin(\theta_i) \neq f_j \sin(\theta_j). \quad (29)$$

Definition 2: The set $\mathcal{M}_2$ contains all signals $u(t)$, such that the support of the Fourier transform $U(f)$ is contained within a union of M disjoint intervals in $\mathcal{F}$. Each of the bandwidths does not exceed B and the transmissions composing $u(t)$ are wide-sense stationary, zero mean and uncorrelated and have unknown and distinct AOAs $|\theta_i| < 90°$, such that (29) holds.

In this section, we wish to design a sampling and reconstruction system which allows for perfect blind signal reconstruction, i.e. recovery of $\boldsymbol{\theta}$, $\boldsymbol{f}$ and $\mathbf{s}(t)$, where $\boldsymbol{\theta}$ denotes the AOAs vector defined above and $\boldsymbol{f}$ and $\mathbf{s}(t)$ are defined in Section II, without any prior knowledge on these.

B. CaSCADE System Description

Each transmission $s_i(t)$ impinges on an L-shaped array with $2N-1$ sensors (N sensors along the x axis and N sensors along the z axis including a common sensor at the origin) in the xz plane with its corresponding AOA θ_i, as shown in Fig. 6. All the sensors have the same sampling pattern as described in Section III-A. In the following sections, we demonstrate that in this case the minimal number of sensors required is $2M+1$. This leads to a minimal sampling rate of $(2M+1)B$ which is assumed to be less than f_{Nyq}. The number of sensors is one more than in the case of known θ_i, but the minimal sampling rate at each channel is the same.

By treating the L-shaped array as two orthogonal ULAs, one along the x axis and the other along the z axis, we form two systems of equations, following the derivations of Section III-B. For the ULA along the x axis, we obtain

$$\mathbf{X}(f) = \mathbf{A}_x \mathbf{W}(f), \quad f \in \mathcal{F}_s, \quad (30)$$

where

$$\mathbf{A}_x = \begin{bmatrix} e^{j2\pi f_1 \tau_1^x(\theta_1)} & \cdots & e^{j2\pi f_M \tau_1^x(\theta_M)} \\ \vdots & & \vdots \\ e^{j2\pi f_1 \tau_N^x(\theta_1)} & \cdots & e^{j2\pi f_M \tau_N^x(\theta_M)} \end{bmatrix}. \quad (31)$$

Similarly, along the z axis,

$$\mathbf{Z}(f) = \mathbf{A}_z \mathbf{W}(f), \quad f \in \mathcal{F}_s, \quad (32)$$

where $\mathbf{A}_z$ is defined accordingly. Here, $\tau_n^x(\theta) = \frac{dn}{c}\cos(\theta)$ and $\tau_n^z(\theta) = \frac{dn}{c}\sin(\theta)$. The matrices $\mathbf{A}_x$ and $\mathbf{A}_z$ depend on both the unknown carrier frequencies $\boldsymbol{f}$ and the AOAs $\boldsymbol{\theta}$, namely

$\mathbf{A}_x = \mathbf{A}_x(\boldsymbol{f}, \boldsymbol{\theta})$ and $\mathbf{A}_z = \mathbf{A}_z(\boldsymbol{f}, \boldsymbol{\theta})$. In the time domain,

$$\mathbf{y}[k] = \begin{bmatrix} \mathbf{x}[k] \\ \mathbf{z}[k] \end{bmatrix} = \mathbf{A}\mathbf{w}[k], \ k \in \mathbb{Z}, \ \mathbf{A} = \begin{bmatrix} \mathbf{A}_x \\ \mathbf{A}_z \end{bmatrix}, \quad (33)$$

where $\mathbf{x}[k]$ and $\mathbf{z}[k]$ are the samples for the x and z axis, respectively, and $\mathbf{w}[k]$ is a vector of length M with ith element $w_i[k]$. In the following sections, we discuss two possible methods to recover $\boldsymbol{f}$ and $\boldsymbol{\theta}$, present sufficient conditions to recover the transmissions $\mathbf{s}(t)$ from $\mathbf{w}[k]$, and provide concrete reconstruction algorithms.

C. Joint ESPRIT Recovery

Our first approach is to extend ESPRIT to a 2D setting, in order to jointly recover f_i and θ_i, for each transmission. Once these are estimated, the transmissions $s_i(t)$ can be recovered from (23) and (19) with the observation matrix $\mathbf{A}$ and the concatenated vector of measurements $\mathbf{y}[k]$ defined in (33).

Consider two sub-arrays of size $N-1$ along each of the x and z axis. The first sub-array along the x axis consists of sensors $\{1, \ldots, N-1\}$. The second sub-array is composed of the last $N-1$ sensors along the same axis, i.e. sensors $\{2, \ldots, N\}$. The sub-arrays along the z axis are similarly defined. Dropping the time variable k for clarity, we have

$$\begin{aligned} \mathbf{x}_1 &= \mathbf{A}_{x_1}\mathbf{w}, \qquad \mathbf{x}_2 = \mathbf{A}_{x_2}\mathbf{w} \\ \mathbf{z}_1 &= \mathbf{A}_{z_1}\mathbf{w}, \qquad \mathbf{z}_2 = \mathbf{A}_{z_2}\mathbf{w}, \end{aligned} \quad (34)$$

where $\mathbf{x}_1$ and $\mathbf{A}_{x_1}$ are the first $N-1$ rows of $\mathbf{x}$ and $\mathbf{A}_x$ respectively and $\mathbf{x}_2$ and $\mathbf{A}_{x_2}$ are the last $N-1$ rows of $\mathbf{x}$ and $\mathbf{A}_x$, respectively. The vectors $\mathbf{z}_1, \mathbf{z}_2$ and matrices $\mathbf{A}_{z_1}, \mathbf{A}_{z_2}$ are defined similarly.

Each couple of sub-array matrices along the same axis are related as follows:

$$\begin{aligned} \mathbf{A}_{x_2} &= \mathbf{A}_{x_1}\boldsymbol{\Phi}, \\ \mathbf{A}_{z_2} &= \mathbf{A}_{z_1}\boldsymbol{\Psi}, \end{aligned} \quad (35)$$

where

$$\begin{aligned} \boldsymbol{\Phi} &\triangleq \operatorname{diag}\left[e^{j2\pi f_1 \tau_1^x(\theta_1)} \ \cdots \ e^{j2\pi f_M \tau_1^x(\theta_M)} \right], \\ \boldsymbol{\Psi} &\triangleq \operatorname{diag}\left[e^{j2\pi f_1 \tau_1^z(\theta_1)} \ \cdots \ e^{j2\pi f_M \tau_1^z(\theta_M)} \right]. \end{aligned} \quad (36)$$

We can see from (36) that the carrier frequencies f_i and AOAs θ_i are embedded in the diagonal matrices $\boldsymbol{\Phi}$ and $\boldsymbol{\Psi}$. Our goal is thus to jointly recover these matrices in order to be able to pair the corresponding elements $f_i\tau_1^x(\theta_i)$ and $f_i\tau_1^z(\theta_i)$. Once $\boldsymbol{\Phi}$ and $\boldsymbol{\Psi}$ are found, the pairs (f_i, θ_i) are calculated as:

$$\theta_i = \tan^{-1}\left(\frac{\angle\Psi_{ii}}{\angle\Phi_{ii}}\right), \quad f_i = \frac{\angle\Phi_{ii}}{2\pi\frac{d}{c}\cos(\theta_i)}, \quad i = 1, \cdots, M. \quad (37)$$

To find $\boldsymbol{\Phi}$ and $\boldsymbol{\Psi}$, we apply the ESPRIT framework to cross-correlation matrices between the sub-arrays of both axis. Consider the following correlation matrices:

$$\begin{aligned} \mathbf{R}_1 &\triangleq \mathbb{E}\left[\mathbf{x}_1\mathbf{z}_1^H\right] = \mathbf{A}_{x_1}\mathbf{R}_w\mathbf{A}_{z_1}^H, \\ \mathbf{R}_2 &\triangleq \mathbb{E}\left[\mathbf{x}_2\mathbf{z}_1^H\right] = \mathbf{A}_{x_2}\mathbf{R}_w\mathbf{A}_{z_1}^H = \mathbf{A}_{x_1}\boldsymbol{\Phi}\mathbf{R}_w\mathbf{A}_{z_1}^H, \\ \mathbf{R}_3 &\triangleq \mathbb{E}\left[\mathbf{x}_1\mathbf{z}_2^H\right] = \mathbf{A}_{x_1}\mathbf{R}_w\mathbf{A}_{z_2}^H = \mathbf{A}_{x_1}\mathbf{R}_w\boldsymbol{\Psi}^H\mathbf{A}_{z_1}^H. \end{aligned} \quad (38)$$

Since the transmissions $s_i(t)$ are assumed to be uncorrelated, $\mathbf{R}_w$ is diagonal. In addition, since $\sigma_i^2 \neq 0$, $(\mathbf{R}_w)_{ii} \triangleq \mathbb{E}\left[w_i^2[k]\right] \neq 0$ and $\mathbf{R}_w$ is invertible. Using the fact that $\boldsymbol{\Psi}^H$ is diagonal as well, we have

$$\mathbf{R}_3 = \mathbf{A}_{x_1}\mathbf{R}_w\boldsymbol{\Psi}^H\mathbf{A}_{z_1}^H = \mathbf{A}_{x_1}\boldsymbol{\Psi}^H\mathbf{R}_w\mathbf{A}_{z_1}^H. \quad (39)$$

Define the concatenated covariance matrix

$$\mathbf{R} = \begin{bmatrix} \mathbf{R}_1 \\ \mathbf{R}_2 \\ \mathbf{R}_3 \end{bmatrix} = \mathbf{B}\mathbf{R}_w\mathbf{A}_{z_1}^H, \qquad \mathbf{B} = \begin{bmatrix} \mathbf{A}_{x_1} \\ \mathbf{A}_{x_1}\boldsymbol{\Phi} \\ \mathbf{A}_{x_1}\boldsymbol{\Psi}^H \end{bmatrix}. \quad (40)$$

The matrices $\boldsymbol{\Phi}, \boldsymbol{\Psi}$ are found using the SVD decomposition of $\mathbf{R}$ as described in Algorithm 2.

In Proposition 2 we show that $\mathbf{R}$ has full column rank, making the solution $\boldsymbol{\Psi}, \boldsymbol{\Phi}$ unique. The SVD of $\mathbf{R}$ then yields

$$\mathbf{R} = [\mathbf{U}_1\mathbf{U}_2]\begin{bmatrix} \boldsymbol{\Lambda} & \mathbf{0} \\ \mathbf{0} & \mathbf{0} \end{bmatrix}\mathbf{V}^H. \quad (41)$$

The columns of the matrix $[\mathbf{U}_1\mathbf{U}_2]$ are the left singular vectors of $\mathbf{R}$, with $\mathbf{U}_1$ containing the vectors corresponding to the first M singular values, $\boldsymbol{\Lambda}$ is a $M \times M$ diagonal matrix with the M non zero singular values of $\mathbf{R}$, and $\mathbf{V}$ contains the right singular vectors of $\mathbf{R}$. Our goal is to obtain $\boldsymbol{\Psi}, \boldsymbol{\Phi}$ from $\mathbf{U}_1$. To this end, we first show that there exists an invertible $M \times M$ matrix $\mathbf{T}$ such that

$$\mathbf{U}_1 = \begin{bmatrix} \mathbf{U}_{11} \\ \mathbf{U}_{12} \\ \mathbf{U}_{13} \end{bmatrix} = \mathbf{B}\mathbf{T}, \quad (42)$$

where $\mathbf{U}_{1i}$ are $(N-1) \times M$ matrices. Proposition 2 provides sufficient conditions for such a $\mathbf{T}$ to exist.

Proposition 2: Let $u(t)$ be an arbitrary signal within $\mathcal{M}_2$ and consider an L-shaped ULA with N sensors and distance d between two adjacent sensors. If:

- (c1) $d \leq \frac{c}{f_{\text{Nyq}}}$
- (c2) $N > M$

then there exists an invertible $M \times M$ matrix $\mathbf{T}$ such that (42) holds.

Proof: We begin by showing that under conditions (c1)–(c2), $\mathbf{R}$ is full column rank. Note that $\mathbf{A}_{x_1}$ and $\mathbf{A}_{z_1}$ are $(N-1) \times M$ Vandermonde matrices, and from (29) and condition (c1), they have distinct columns. Hence, given condition (c2), $\mathbf{A}_{x_1}$ and $\mathbf{A}_{z_1}$ are full column rank. The $M \times M$ matrix $\mathbf{R}_w$ is diagonal and invertible. It follows that $\mathbf{R}_1, \mathbf{R}$ and $\mathbf{B}$ are full column rank.

The SVD decomposition of $\mathbf{R}$ yields (41). In particular, it holds that $\mathbf{R}^H\mathbf{U}_2 = \mathbf{0}$, so that

$$\mathbf{A}_{z_1}\mathbf{R}_w\mathbf{B}^H\mathbf{U}_2 = \mathbf{0}.$$

Since $\mathbf{A}_{z_1}\mathbf{R}_w$ is full column rank, it follows that $\mathbf{B}^H\mathbf{U}_2 = \mathbf{0}$. Now, $\mathbf{B}$ and $\mathbf{U}_1$ are both $3(N-1) \times M$ matrices, with column rank M. In addition, the $3(N-1) \times (3(N-1) - M)$

matrix $\mathbf{U}_2$ is in the null space of $\mathbf{B}^H$ and $\mathbf{U}_1^H$. This implies that range $(\mathbf{B})$ = range $(\mathbf{U}_1)$. Therefore, there exists an $M \times M$ invertible matrix $\mathbf{T}$ such that (42) holds. ■

If the conditions of Proposition 2 hold, then we can write

$$\begin{aligned} \mathbf{A}_{x_1} &= \mathbf{U}_{11}\mathbf{T}^{-1} \\ \mathbf{U}_{12} &= \mathbf{A}_{x_1}\boldsymbol{\Phi}\mathbf{T} = \mathbf{U}_{11}\mathbf{T}^{-1}\boldsymbol{\Phi}\boldsymbol{T} \\ \mathbf{U}_{13} &= \mathbf{A}_{x_1}\boldsymbol{\Psi}^H\mathbf{T} = \mathbf{U}_{11}\mathbf{T}^{-1}\boldsymbol{\Psi}^H\mathbf{T}. \end{aligned} \tag{43}$$

In addition, since the $(N-1)\times M$ matrix $\mathbf{U}_{11}$ satisfies $\mathbf{U}_{11} = \mathbf{A}_{x_1}\mathbf{T}$, where $\mathbf{T}$ is invertible and rank$(\mathbf{A}_{x_1}) = M$, we have that rank$(\mathbf{U}_{11}) = M$ and $\mathbf{U}_{11}^{\dagger}\mathbf{U}_{11} = \mathbf{I}$.

Applying $\mathbf{U}_{11}^{\dagger}$ on the left of (43) we get

$$\begin{aligned} \mathbf{U}_{11}^{\dagger}\mathbf{U}_{12} &= \mathbf{T}^{-1}\boldsymbol{\Phi}\boldsymbol{T} \\ \mathbf{U}_{11}^{\dagger}\mathbf{U}_{13} &= \mathbf{T}^{-1}\boldsymbol{\Psi}^H\mathbf{T}. \end{aligned} \tag{44}$$

Therefore, we can obtain $\boldsymbol{\Phi}$ and $\mathbf{T}$ using the eigenvalue decomposition of $\mathbf{U}_{11}^{\dagger}\mathbf{U}_{12}$, up to permutation. Denote by $\hat{\boldsymbol{\Phi}}$ and $\hat{\mathbf{T}}$ the resulting matrices. We then compute $\hat{\boldsymbol{\Psi}}$ with the same permutation as

$$\hat{\boldsymbol{\Psi}}^H = \hat{\mathbf{T}}(\mathbf{U}_{11}^{\dagger}\mathbf{U}_{13})\hat{\mathbf{T}}^{-1}. \tag{45}$$

If (45) is not diagonal, due to numerical errors or noise, then we approximate it by taking only the diagonal elements of (45). Since the electronic angles $f_i \cos(\theta_i)$ and $f_i \sin(\theta_i)$ are distinct, the eigenvalues of $\hat{\boldsymbol{\Phi}}$ and $\hat{\boldsymbol{\Psi}}$ are distinct as well and it follows that both matrices have the same permutation. We thus obtain proper pairing between the diagonal elements. The AOAs θ_i and carrier frequencies f_i are then given by (37).

Algorithm 2 summarizes the main steps of the joint 2D ESPRIT described above. In the algorithm description we exploit the 4 cross-correlation matrices between the sub-arrays instead of only 3 as defined in (38) to increase robustness to noise. In our derivations, we assumed perfect knowledge of $\mathbf{R}$. In practice, it is estimated from Q snapshots, as shown in Algorithm 2.

Theorem 4 summarizes sufficient conditions for perfect blind reconstruction of $\boldsymbol{f}$ and $\boldsymbol{\theta}$ from the low rate samples $\mathbf{x}[k]$ and $\mathbf{z}[k]$.

Theorem 4: Let $u(t)$ be an arbitrary signal within $\mathcal{M}_2$. Consider an L-shaped ULA with $2N-1$ sensors, such that there are N sensors along each axis with a common sensor at the origin. Denote the distance between two adjacent sensors by d. If:

- (c1) $d < \frac{c}{f_{\text{Nyq}}}$
- (c2) $N > M$,

then (30)–(32) has a unique solution $(\boldsymbol{f}, \boldsymbol{\theta}, \mathbf{w})$.

Proof: From Proposition 2, under conditions (c1)–(c2), $\mathbf{U}_{11}$ is full column rank and thus left invertible. Therefore, $\boldsymbol{\Phi}$ and $\boldsymbol{\Psi}$ can be uniquely derived from (44), with the same permutation $\mathbf{T}$ for both matrices. This follows from the assumption that the electronic angles, and as a consequence the eigenvalues of $\boldsymbol{\Phi}$ and $\boldsymbol{\Psi}$, are distinct. Condition (c1) implies that both $2\pi\hat{f}_i\frac{d}{c}\cos(\hat{\theta}_i) \in (-\pi, \pi]$ and $2\pi\hat{f}_i\frac{d}{c}\sin(\hat{\theta}_i) \in (-\pi, \pi]$ namely $\angle\Psi_{i,i}$ and $\angle\Phi_{i,i}$, for $1 \le i \le M$, are unique. Therefore, $\boldsymbol{f}, \boldsymbol{\theta}$ are unique as well and given by (37). Using (31) to compute $\mathbf{A}_x$ and $\mathbf{A}_z$ we can construct $\mathbf{A}$ as in (33) and $\mathbf{w}$ is uniquely determined by $\mathbf{w} = \mathbf{A}^{\dagger}\mathbf{y}$. ■

In addition, if conditions (c1)–(c2) from Theorem 2 hold, then $s_i(t)$ is uniquely recovered from $\mathbf{x}[k]$ and $\mathbf{z}[k]$ using (23) and (19) with the observation matrix $\mathbf{A}$.

From Theorem 4, the minimal necessary number of sensors in each axis, including a common sensor at the origin, to allow perfect blind reconstruction is $N \ge M+1$. This leads to a total number of sensors $2N-1 \ge 2M+1$. In addition, for perfect reconstruction we require $f_s \ge B$ as in Theorem 2. Thus, the minimal sampling rate is bounded by $(2M+1)B$ using this approach.

Algorithm 2: Joint ESPRIT.

Input:

- Q snapshots of the measurements $\mathbf{x}$ along the x axis
- Q snapshots of the measurements $\mathbf{z}$ along the z axis

Output:

- $\hat{\boldsymbol{f}}$ - estimated carriers frequencies
- $\hat{\boldsymbol{\theta}}$ - estimated AOAs

Algorithm:

1) Define $\mathbf{x}_1$ and $\mathbf{x}_2$ as the first and last $N-1$ rows of $\mathbf{x}$ Define $\mathbf{z}_1$ and $\mathbf{z}_2$ as the first and last $N-1$ rows of $\mathbf{z}$
2) Estimate the cross covariance matrices:
   a) $\mathbf{R}_1 = \sum_{k=1}^{Q}\mathbf{x}_1[k]\mathbf{z}_1^H[k]$
   b) $\mathbf{R}_2 = \sum_{k=1}^{Q}\mathbf{x}_2[k]\mathbf{z}_1^H[k]$
   c) $\mathbf{R}_3 = \sum_{k=1}^{Q}\mathbf{x}_1[k]\mathbf{z}_2^H[k]$
   d) $\mathbf{R}_4 = \sum_{k=1}^{Q}\mathbf{x}_2[k]\mathbf{z}_2^H[k]$
3) Decompose $\mathbf{R} = \begin{bmatrix}\mathbf{R}_1^T & \mathbf{R}_2^T & \mathbf{R}_3^T & \mathbf{R}_4^T\end{bmatrix}^T$ using the SVD: $\mathbf{R} = \mathbf{U}\boldsymbol{\Sigma}\mathbf{V}^H$
4) Set $\mathbf{U}_1$ to be the $(4N-4)\times M$ matrix that contains the M left singular vectors corresponding to the largest singular values of $\mathbf{R}$
5) Define:
   a) $\mathbf{U}_{11}$ as the first $N-1$ rows of $\mathbf{U}$
   b) $\mathbf{U}_{12}$ as the next $N-1$ rows of $\mathbf{U}$
   c) Same for $\mathbf{U}_{13}$, $\mathbf{U}_{14}$
6) Compute:
   a) $\mathbf{V}_1 = \mathbf{U}_{11}^{\dagger}\mathbf{U}_{12}$
   b) $\mathbf{V}_2 = \mathbf{U}_{11}^{\dagger}\mathbf{U}_{13}$
   c) $\mathbf{V}_3 = \mathbf{U}_{11}^{\dagger}\mathbf{U}_{14}$
7) Perform an eigenvalue decomposition of $\frac{1}{3}(\mathbf{V}_1 + \mathbf{V}_2 + \mathbf{V}_3) = \mathbf{T}\boldsymbol{\Lambda}\mathbf{T}^{-1}$, where $\boldsymbol{\Lambda}$ is a diagonal matrix
8) Compute $\hat{\boldsymbol{\Phi}} = \mathbf{T}^{-1}\mathbf{V}_1\mathbf{T}$ and $\hat{\boldsymbol{\Psi}} = \left(\mathbf{T}^{-1}\mathbf{V}_2\mathbf{T}\right)^H$
9) Compute the carrier frequencies and AOAs using (37)

D. CS Approach

In this section, we derive an alternative joint carrier frequency and AOA recovery approach based on CS methods. Consider the measurements $\mathbf{y}[k]$ as in (33), and their correlation matrix

$$\mathbf{R} = \mathbb{E}\left[\mathbf{y}[k]\mathbf{y}^H[k]\right] = \mathbf{A}\mathbf{R}_w\mathbf{A}^H, \tag{46}$$

with $\mathbf{A}$ as in (33). In the following, we assume perfect knowledge of $\mathbf{R}$. In practice, it can be estimated from Q snapshots of $\mathbf{y}[k]$ as $\mathbf{R} = \sum_{k=1}^{Q} \mathbf{y}[k]\mathbf{y}[k]^H$.

Denote $\alpha_i = f_i \cos\theta_i$ and $\beta_i = f_i \sin\theta_i$ and suppose that α_i and β_i lie on a grid $\{\delta l\}_{l=-L_0}^{L_0}$, with $L_0 = \frac{f_{\text{Nyq}}}{2\delta}$. As in Section III-D2, δ defines the grid resolution. We can then write (46) as

$$\mathbf{R} = \mathbf{G}\mathbf{R}_w^g\mathbf{G}^H, \tag{47}$$

where $\mathbf{G}$ is a $(2N-1) \times L^2$ matrix with (n,l)th element $G_{nl} = e^{j2\pi \frac{dn}{c}\alpha_{l_1}}$, for $0 \le n \le N-1$ and $G_{nl} = e^{j2\pi \frac{d(n-N+1)}{c}\beta_{l_2}}$, for $N \le n \le 2N-1$. Here, $L = 2L_0+1$, $l_1 = (l \mod L) - L_0$ and $l_2 = \lfloor \frac{l}{L} \rfloor - L_0$. The nonzero elements of the $L^2 \times L^2$ matrix $\mathbf{R}_w^g$ are the M diagonal elements of $\mathbf{R}_w$ at the M indices corresponding to $\{\alpha_i, \beta_i\}$. With high probability, the discretization conserves the unambiguous property, namely $\text{spark}(\mathbf{G}) = N+1$. Formulating concrete conditions to ensure the lack of ambiguity is very involved and thus this property is traditionally assumed without justification [37].

Since $\mathbf{R}_w^g$ is diagonal, the observation model (47) can be equivalently written in vector form as

$$\text{vec}(\mathbf{R}) = \left(\bar{\mathbf{G}} \odot \mathbf{G}\right)\mathbf{r}_w^g. \tag{48}$$

Here, $\text{vec}(\mathbf{R})$ is a column vector that vectorizes the matrix $\mathbf{R}$ by stacking its columns, $\mathbf{r}_w^g$ is the $L^2 \times 1$ vector that contains the diagonal of $\mathbf{R}_w^g$ and $\odot$ denotes the Khatri-Rao product. Our goal is thus to recover the M-sparse vector $\mathbf{r}_w^g$ from the $(2N-1)^2$ measurement vector $\text{vec}(\mathbf{R})$.

The following theorem derives a necessary condition on the minimal number of sensors $2N-1$ for perfect recovery of $\alpha_i, \beta_i, i \in \{1, \ldots, M\}$ in a noiseless environment.

Theorem 5: Let $u(t)$ be an arbitrary signal within $\mathcal{M}_2$. Consider an L-shaped ULA with $2N-1$ sensors, such that there are N sensors along each axis with a common sensor at the origin. Denote the distance between two adjacent sensors by d. If:

- (c1) $d < \frac{c}{f_{\text{Nyq}}}$
- (c2) $N > M$
- (c3) $\text{spark}(\mathbf{G}) = N+1$,

then (48) has a unique M-sparse solution $\mathbf{r}_w^g$.

Proof: In order to recover the M-sparse vector $\mathbf{r}_w^g$ from $\text{vec}(\mathbf{R})$, we require [26], [33]

$$\text{spark}\left(\bar{\mathbf{G}} \odot \mathbf{G}\right) > 2M. \tag{49}$$

From [39], it holds that

$$\text{spark}\left(\bar{\mathbf{G}} \odot \mathbf{G}\right) \ge \min\{2(\text{spark}(\mathbf{G})-1), L^2+1\}. \tag{50}$$

Combining (c2) and (c3), we have

$$2(\text{spark}(\mathbf{G})-1) > 2M. \tag{51}$$

Finally, since $L^2 \gg N$, (49) holds. ■

To recover the sparse vector $\mathbf{r}_w^g$, we can use any CS recovery algorithm [26]. Once the indices $\alpha_i, \beta_i,\ i \in \{1, \ldots, M\}$ are found, and assuming condition (c1), the corresponding f_i and θ_i are given uniquely by

$$\hat{\theta}_i = \tan^{-1}\left(\frac{\beta_i}{\alpha_i}\right), \quad \hat{f}_i = \frac{\alpha_i}{\cos(\theta_i)}. \tag{52}$$

We conclude by noting that both ESPRIT and OMP are widely used algorithms whose complexity analysis has been explored in the literature. We did not optimize the algorithms in terms of computational load, and more efficient implementations may be used for this purpose.

V. Numerical Experiments

We now numerically investigate different aspects of our systems. First we consider the spectrum sensing problem presented in Section II, and compare the performance of our ULA scheme, shown in Fig. 3 with that of the MWC [23] of Fig. 2. We show that at low SNRs, we outperform the MWC in terms of recovery error. We explore the impact of SNR and number of sensors/channels N on the signal reconstruction performance for both architectures. We then move on to the joint spectrum sensing and DOA estimation problem as presented in Section IV. We investigate the performance of our system in terms of frequencies and AOAs recovery error as a function of SNR and number of sensors.

A. Spectrum Sensing

We begin by considering the spectrum sensing problem of Section II. The setup described hereafter is used as a basis for all simulations. Consider signals of the model $\mathcal{M}_1$ with $M = 3$, $f_{\text{Nyq}} = 10$ GHz, $\theta = 0^\circ$ and $B = 50$ MHz. The carrier frequencies f_i are drawn uniformly at random from $[-\frac{f_{\text{Nyq}}-B}{2}, \frac{f_{\text{Nyq}}-B}{2}]$. In our ULA based system, the received signal at each sensor is given by (4), and is corrupted by additive white Gaussian noise (AWGN), uncorrelated between the different sensors. For the MWC system, the received signal at the single sensor is the sum of the transmissions with AWGN, that is then split to the different MWC channels. Here, all channels are corrupted by the same noise. Both system noises have the same variance.

In all the simulations, we use $f_s = f_p = 1.3B$. For the ULA based system, we use a periodic function $p(t)$ such that $P(f) = \sum_{l=-\infty}^{\infty} \delta(f - lf_p)$. In the MWC, $p_i(t)$ are chosen as piecewise constant functions alternating between the levels ± 1 with sequences generated uniformly at random. Performance is measured by computing the MSE between the original and reconstructed signals, i.e. $\text{MSE} = \frac{||u-\hat{u}||^2}{||u||^2}$. In the simulations, we estimate the correlation matrix as $\mathbf{R} = \sum_{k=1}^{Q} \mathbf{x}[k]\mathbf{x}^H[k]$.

To set similar conditions for both systems (MWC and ULA), we use the same parameters, i.e the number of source signals M, number of snapshots Q, SNR, f_p, f_s, and N, which in the ULA denotes the sensors number and in the MWC the channels number. Note that both systems require the same minimal number of channels given in condition (c1) in Theorem 1 for the ULA and equal to $N \ge 2M - \dim(\text{span}(\mathbf{w}))$ [23]. For the ULA based system, we show both the MMV CS approach, using SOMP [26], and ESPRIT approach, described in Section III-D.

Fig. 7 presents the performance of the ULA based system as a function of d. As shown in Theorem 1, we require $d \le \frac{c}{|\cos(\theta)| \cdot f_{\text{Nyq}}}$, which in our setting translates to $d \le \frac{3 \cdot 10^8}{10^{10}} = 0.03[m]$. This property of the system geometry is clearly demonstrated in the figure, where we observe a monotonic decrease

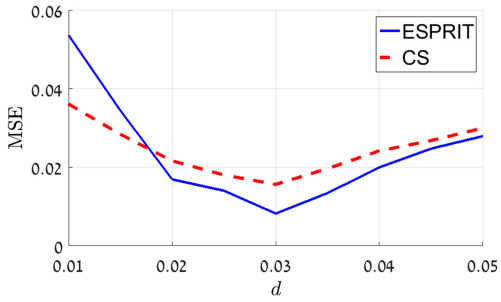

Fig. 7. Influence of the distance d between adjacent sensors. with $M = 3$, $N = 10$, $Q = 400$, and SNR $= 10$ dB.

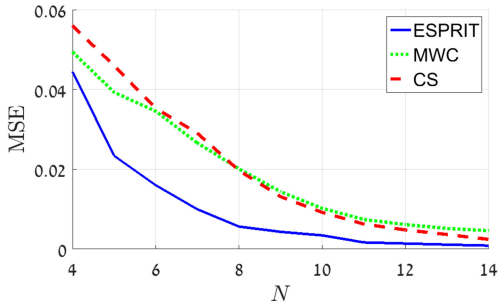

Fig. 8. Influence of the number of sensors N, with $M = 3$, $Q = 300$, SNR $=$ 10 dB.

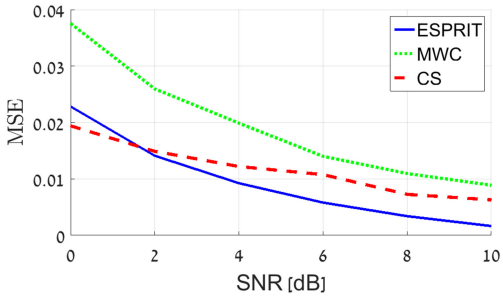

Fig. 9. Influence of SNR, with $M = 3$, $N = 10$, $Q = 300$.

in performance starting from $d = 0.03$, for both reconstruction methods, MMV and ESPRIT. In the following simulations, d is set to $d = 0.03$.

The next experiment examines the influence of the number of sensors N. A large amount of sensors increases the system's robustness to noise and allows it to handle a greater amount of source signals. This parameter is equivalent to the number of channels in the MWC. From Fig. 8, it can be seen that the reconstruction error decreases with more sensors.

In Fig. 9, we examine the reconstruction performance under different SNR conditions. The simulations demonstrate that our system outperforms the MWC, in particular in low SNR regimes. In addition, in such settings, CS recovery outperforms ESPRIT as expected. With increasing SNR, the recovery error of ESPRIT decreases below that of CS. This is due to the fact that CS recovery is limited to a predefined grid and the signal carriers were not generated on a specific grid. Thus, in high SNR

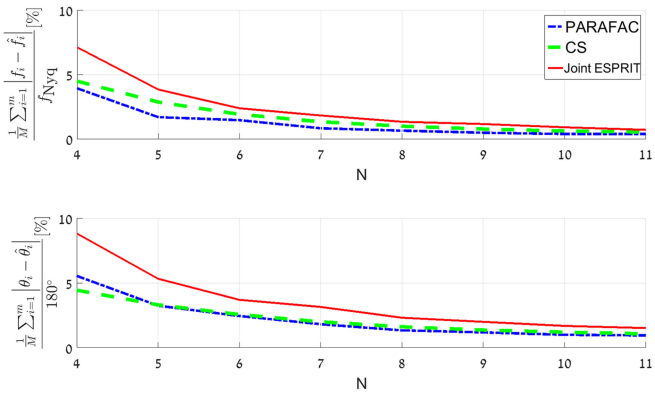

Fig. 10. Influence of the number of sensors $2N - 1$, with $M = 3$, $Q = 300$, SNR $= 10$ dB.

regimes, ESPRIT outperform CS due to off grid errors of the latter. In the presence of enough samples, obtained by increasing the sampling rate f_s, the number of sensors N or snapshots Q, ESPRIT achieves better results.

B. Joint Spectrum Sensing and DOA Recovery

We next demonstrate the effect of different system parameters on the joint spectrum sensing and DOA recovery performance. Consider a complex-valued signal $u(t)$ from $\mathcal{M}_2$, with similar parameters as above, and AOAs θ_i drawn uniformly at random from $[-85^\circ, 85^\circ]$. The L-shaped array is composed of $2N - 1$ sensors; N along each axis with a common sensor at the origin. The received signal at each sensor in the L-shaped array is corrupted with AWGN. The mixing and sampling rates are set to $f_s = f_p = 1.4B$.

We compare 3 reconstruction methods: 1) Joint ESPRIT summarized in Algorithm 2, 2) CS approach presented in Section IV-D, 3) PARAFAC [27] based approach, as presented in [30]. PARAFAC extends the bilinear model of factor analysis to a trilinear model using the alternating least squares (ALS) method. In [30], it is used to decompose the cross correlations matrices defined in (38) into three matrices, isolating $\mathbf{\Phi}$ and $\mathbf{\Psi}$. To apply the PARAFAC algorithm we use the COMFAC MATLAB function implemented by [40].

In these simulations, we focus on the recovery of the carrier frequencies f_i and AOAs θ_i. Once these are recovered, full signal reconstruction can be performed as shown in the first part of this work (see (23) and (19)). The reconstruction performance is measured by the following criteria: $\frac{1}{M f_{\text{Nyq}}} \sum_{i=1}^{m} |f_i - \hat{f}_i|$ for the frequencies, and $\frac{1}{M 180^\circ} \sum_{i=1}^{m} |\theta_i - \hat{\theta}_i|$ for the AOA. The first simulation examines the recovery performance with respect to the number of sensors $2N - 1$. Fig. 10 presents the carrier frequency and AOA reconstruction performance for different values of the number of sensors, which affects both the noise averaging and the total amount of samples available. The second simulation, presented in Fig. 11, illustrates the impact of SNR on the recovery performance.

The figures demonstrate similar behavior of CS and ESPRIT as in the previous section. The PARAFAC algorithm, which is

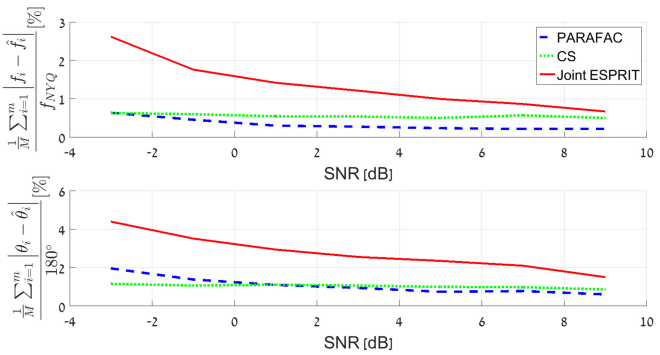

Fig. 11. Influence of SNR, with $M = 3$, $2N - 1 = 11$, $Q = 300$.

more computationally complex and requires several iterations, is shown to outperform both joint ESPRIT and CS except in the regime of low SNR and small number of sensors. This stems from the fact that PARAFAC does not fully exploit the problem's structure [30] and therefore, its performance decreases with few or noisy measurements.

VI. Conclusion

In this paper, we considered two spectrum sensing scenarios of multiband signals from sub-Nyquist samples: we first examined the task of frequency spectrum sensing and then extended our approach to joint spectrum sensing and DOA recovery. For the first scenario, we proposed a receiver composed of a ULA, where each sensor contains an analog front-end equivalent to one channel of the MWC. This system constitutes an alternative sub-Nyquist sampling scheme that outperforms the MWC in terms of performance in low SNR regimes and is less complex to implement. For the joint spectrum sensing and DOA recovery scenario, we extended our ULA configuration and presented the CaSCADE system, an L-shaped array composed of two ULAs with the same sampling scheme as above. In both cases, we derived sufficient conditions for the recovery of the transmissions carrier frequencies and AOAs, if relevant. We showed that the minimal number of sensors for the first scenario is twice the number of transmissions, namely $2M$, in the worst case and $M + 1$ with high probability, whereas in the second scenario, it is $2M + 1$ in the average case. Last, we provided two reconstruction schemes for both scenarios: one based on the analytic method ESPRIT and the second based on CS techniques. Simulations demonstrated the performance of the above algorithms in comparison with existing methods.

References

[1] H. Urkowitz, "Energy detection of unknown deterministic signals," *Proc. IEEE*, vol. 55, no. 4, pp. 523–531, Apr. 1967.

[2] G. L. Turin, "An introduction to matched filters," *IRE Trans. Inf. Theory*, vol. 6, pp. 311–329, Jun. 1960.

[3] W. A. Gardner, A. Napolitano, and L. Paura, "Cyclostationarity: Half a century of research," *Signal Process.*, vol. 86, pp. 639–697, 2006.

[4] V. F. Pisarenko, "The retrieval of harmonics from a covariance function," *Geophys., J. Roy. Astron. Soc.*, vol. 33, pp. 347–366, 1973.

[5] R. O. Schmidt, "Multiple emitter location and signal parameter estimation," *IEEE Trans. Antennas Propag.*, vol. 34, no. 3, pp. 276–280, Mar. 1986.

[6] R. Roy and T. Kailath, "ESPRIT-estimation of signal parameters via rotational invariance techniques," *IEEE Trans. Signal Process.*, vol. 37, no. 7, pp. 984–995, Jul. 1989.

[7] G. Xu and T. Kailath, "Fast subspace decomposition," *IEEE Trans. Signal Process.*, vol. 42, no. 3, pp. 539–551, Mar. 1994.

[8] J. Xin and A. Sano, "Computationally efficient subspace-based method for direction-of-arrival estimation without eigendecomposition," *IEEE Trans. Signal Process.*, vol. 52, no. 4, pp. 876–893, Mar. 2004.

[9] J. Mitola, "Software radios: Survey, critical evaluation and future directions," *IEEE Aerosp. Electron. Syst. Mag.*, vol. 8, no. 4, pp. 25–36, Apr. 1993.

[10] FCC, "Spectrum policy task force report: Federal communications commission," FCC, Washington, DC, USA, Tech. Rep. 02–135. [Online]. Available: http://www.gov/edocs_public/attachmatch/DOC228542A1.pdf, Nov. 2002.

[11] M. A. McHenry and D. McCloskey, "Spectrum occupancy measurements, Chicago, Illinois, November 16–18, 2005, Shared Spectrum Company, Tech. Rep.," Project: NeTS-ProWIN: Subcontract No. SA301-0905. [Online]. Available: http://www.sharedspectrum.com, Dec. 2005.

[12] S. Haykin, "Cognitive radio: Brain-empowered wireless communications," *IEEE J. Sel. Areas Commun.*, vol. 23, no. 2, pp. 201–220, Feb. 2005.

[13] A. Ghasemi and E. S. Sousa, "Spectrum sensing in cognitive radio networks: Requirements, challenges and design trade-offs," *IEEE Commun. Mag.*, vol. 46, no. 4, pp. 32–39, Apr. 2008.

[14] M. Mishali and Y. C. Eldar, "Sub-Nyquist sampling: Bridging theory and practice," *IEEE Signal Process. Mag.*, vol. 28, no. 6, pp. 98–124, Nov. 2011.

[15] E. G. Larsson and M. Skoglund, "Cognitive radio in a frequency-planned environment: Some basic limits," *IEEE Trans. Wireless Commun.*, vol. 7, no. 12, pp. 4800–4806, Dec. 2008.

[16] A. Sahai, N. Hoven, and R. Tandra, "Some fundamental limits on cognitive radio," in *Proc. Annu. Allerton Conf. Commun., Control, Comput.*, Oct. 2004, pp. 1662–1671.

[17] J.-F. Gu and P. Wei, "Joint SVD of two cross-correlation matrices to achieve automatic pairing in 2-D angle estimation problems," *IEEE Antennas Wireless Propag. Lett.*, vol. 6, pp. 553–556, 2007.

[18] J.-F. Gu, W.-P. Zhu, and M. N. S. Swamy, "Joint 2-D DOA estimation via sparse L-shaped array," *IEEE Trans. Signal Process.*, vol. 63, no. 1, pp. 1171–1182, Mar. 2015.

[19] A. N. Lemma, A. van der Veen, and E. F. Deprettere, "Joint angle-frequency estimation using multi-resolution ESPRIT estimation," in *Proc. IEEE Int. Conf. Acoust., Speech Signal Process.*, May 1998, pp. 1957–1960.

[20] A. N. Lemma, A. van der Veen, and E. F. Deprettere, "Analysis of joint angle-frequency estimation using ESPRIT," *IEEE J. Sel. Top. Signal Process.*, vol. 51, no. 5, pp. 1264–1283, May 2003.

[21] W. Xudong, X. Zhang, J. Li, and J. Bai, "Improved ESPRIT method for joint direction-of-arrival and frequency estimation using multiple-delay output," *Int. J. Antennas Propag.*, vol. 2012, pp. 1–9, Jul. 2012. doi: 10.1155/2012/309269.

[22] M. Mishali and Y. C. Eldar, "Blind multiband signal reconstruction: Compressed sensing for analog signals," *IEEE Trans. Signal Process.*, vol. 57, no. 3, pp. 993–1009, Mar. 2009.

[23] M. Mishali and Y. C. Eldar, "From theory to practice: Sub-Nyquist sampling of sparse wideband analog signals," *IEEE J. Sel. Topics Signal Process.*, vol. 4, no. 2, pp. 375–391, Apr. 2010.

[24] D. D. Arianandа and G. Leus, "Compressive joint angular-frequency power spectrum estimation," in *Proc. IEEE Eur. Signal Process. Conf.*, Sep. 2013, pp. 1–5.

[25] A. A. Kumar, S. G. Razul, and C. S. See, "An efficient sub-Nyquist receiver architecture for spectrum blind reconstruction and direction of arrival estimation," in *Proc. IEEE Int. Conf. Acoust., Speech Signal Process.*, May 2014, pp. 6781–6785.

[26] Y. C. Eldar and G. Kutyniok, *Compressed Sensing: Theory and Applications*. Cambridge, U.K.: Cambridge Univ. Press, 2012.

[27] R. A. Harshman and M. E. Lundy, "PARAFAC: Parrallel factor analysis," *Comput. Statist. Data Anal.*, vol. 18, no. 1, pp. 39–72, 1994.

[28] Z. Xiaofei, L. Jianfeng, and X. Lingyun, "Novel two-dimensional doa estimation with l-shaped array," *EURASIP J. Adv. Signal Process.*, vol. 2011, no. 50, pp. 1–7, Aug. 2011.

[29] D. Liu and J. Liang, "L-shaped array-based 2-D doa estimation using parallel factor analysis," in *Proc. World Congr. Intell. Control Autom.*, Jul. 2010, pp. 6949–6952.

[30] S. Stein, O. Yair, D. Cohen, and Y. C. Eldar, "Joint spectrum sensing and direction of arrival recovery from sub-Nyquist samples," in *Proc. IEEE Int. Workshop Signal Process. Adv. Wireless Commun.*, Jun. 2015, pp. 331–335.
[31] H. J. Landau, "Necessary density conditions for sampling and interpolation of certain entire functions," *Acta Math*, vol. 117, pp. 37–52, Jul. 1967.
[32] M. Mishali, Y. C. Eldar, O. Dounaevsky, and E. Shoshan, "Xampling: Analog to digital at sub-nyquist rates," *IET Circuits, Dev. Syst.*, vol. 5, no. 1, pp. 8–20, Jan. 2011.
[33] Y. C. Eldar, *Sampling Theory: Beyond Bandlimited Systems*. Cambridge, U.K.: Cambridge Univ. Press, 2015.
[34] K. Gedalyahu and Y. C. Eldar, "Time-delay estimation from low-rate samples: A union of subspaces approach," *IEEE Trans. Signal Process.*, vol. 58, no. 6, pp. 3017–3031, Jun. 2010.
[35] M. Mishali and Y. C. Eldar, "Reduce and boost: Recovering arbitrary sets of jointly sparse vectors," *IEEE Trans. Signal Process.*, vol. 56, no. 1, pp. 4692–4702, Oct. 2008.
[36] M. E. Davies and Y. C. Eldar, "Rank awareness in joint sparse recovery," *IEEE Trans. Inf. Theory*, vol. 58, no. 2, pp. 1135–1146, Feb. 2012.
[37] R. Roy, B. Ottersten, A. L. Swindlehurst, and T. Kailath, "Multi invariance ESPRIT," *IEEE Trans. Signal Process.*, vol. 40, pp. 867–881, Apr. 1992.
[38] S. Kikuchi, H. Tsuji, and A. Sano, "Pair-matching method for estimating 2-D angle of arrival with a cross-correlation matrix," *IEEE Antennas Wireless Propag. Lett.*, vol. 5, pp. 867–881, 2006.
[39] N. D. Sidiropoulos and R. Bro, "On the uniqueness of multilinear decomposition of n-way arrays," *J. Chemometrics*, vol. 14, pp. 229–239, 2000.
[40] N. D. Sidiropoulos, "COMFAC: MATLAB code for LS fitting of the complex PARAFAC model in 3-D," 1998. [Online]. Available: http://www.telecom.tuc.gr/~nikos

Shahar Stein Ioushua (S'15) received the B.Sc. degree in electrical engineering (cum laude) from the Technion—Israel Institute of Technology, Haifa, Israel, in 2015, where she is currently working toward the M.Sc. degree in electrical engineering.

Since 2015, she has been a Teaching Assistant with the Viterbi Faculty of Electrical Engineering and a Project Supervisor with the Signal Acquisition, Modeling and Processing Laboratory (SAMPL), Electrical Engineering Department, Technion. Her research interests include theoretical aspects of signal processing, compressed sensing and signal processing for communication signals.

Mrs. Stein Ioushua received the Meyer Foundation Excellence prize in 2015. She, is an Gutwirth Fellow since 2017.

Or Yair (S'15) received the B.Sc. degree (summa cum laude) in electrical engineering from the Technion—Israel Institute of Technology, Haifa, Israel, in 2015, where he is currently working toward the Ph.D. degree.

From 2012 to 2015, he worked in the field of image processing and algorithms. Since 2015, he has been a Teaching Assistant with the Viterbi Faculty of Electrical Engineering, Technion—Israel Institute of Technology. His main areas of interest include signal processing, machine learning and geometric methods.

Mr. Yair received the Meyer Fellowship and Zipers Award for 2015 and the Diane and Leonard Sherman Interdisciplinary Fellowship for 2016.

Deborah Cohen (S'13) received the B.Sc. degree in electrical engineering (summa cum laude) from the Technion—Israel Institute of Technology, Haifa, Israel, in 2010, where she is currently working toward the Ph.D. degree in electrical engineering.

Since 2010, she has been a Project Supervisor with the Signal and Image Processing Laboratory, the High Speed Digital Systems Laboratory, the Communications Laboratory, and the Signal Acquisition, Modeling and Processing Laboratory,the Electrical Engineering Department, Technion. Her research interests include theoretical aspects of signal processing, sampling theory, compressed sensing, spectrum sensing, signal processing for communication and radar signals.

Ms. Cohen received the Meyer Foundation Excellence prize in 2011, the Sandor Szego Award and the Vivian Konigsberg Award for Excellence in Teaching in 2012. She was awarded the David and Tova Freud and Ruth Freud-Brendel Memorial Scholarship in 2014 and the Jacknow Award for Excellence in Teaching in 2015. She is an Azrieli Fellow since 2014.

Yonina C. Eldar (S'98–M'02–SM'07–F'12) received the B.Sc. degree in physics and the B.Sc. degree in electrical engineering both from Tel-Aviv University (TAU), Tel-Aviv, Israel, in 1995 and 1996, respectively, and the Ph.D. degree in electrical engineering and computer science from the Massachusetts Institute of Technology (MIT), Cambridge, MA, USA, in 2002.

From January 2002 to July 2002, she was a Postdoctoral Fellow at the Digital Signal Processing Group, MIT. She is currently a Professor in the Department of Electrical Engineering, Technion—Israel Institute of Technology, Haifa, Israel, where she holds the Edwards Chair in Engineering. She is also a Research Affiliate with the Research Laboratory of Electronics at MIT and was a Visiting Professor at Stanford University, Stanford, CA, USA. She is the author of the book *Sampling Theory: Beyond Bandlimited Systems* and Coauthor of the books *Compressed Sensing* and *Convex Optimization Methods in Signal Processing and Communications*, all published by Cambridge University Press. Her research interests include the broad areas of statistical signal processing, sampling theory and compressed sensing, optimization methods, and their applications to biology and optics.

Dr. Eldar has received many awards for excellence in research and teaching, including the IEEE Signal Processing Society Technical Achievement Award (2013), the IEEE/AESS Fred Nathanson Memorial Radar Award (2014), and the IEEE Kiyo Tomiyasu Award (2016). She was a Horev Fellow of the Leaders in Science and Technology program at the Technion and an Alon Fellow. She received the Michael Bruno Memorial Award from the Rothschild Foundation, the Weizmann Prize for Exact Sciences, the Wolf Foundation Krill Prize for Excellence in Scientific Research, the Henry Taub Prize for Excellence in Research (twice), the Hershel Rich Innovation Award (three times), the Award for Women with Distinguished Contributions, the Andre and Bella Meyer Lectureship, the Career Development Chair at the Technion, the Muriel & David Jacknow Award for Excellence in Teaching, and the Technions Award for Excellence in Teaching (two times). She received several best paper awards and best demo awards together with her research students and colleagues including the SIAM outstanding Paper Prize, the UFFC Outstanding Paper Award, the Signal Processing Society Best Paper Award and the IET Circuits, Devices and Systems Premium Award, and was selected as one of the 50 most influential women in Israel. She is a member of the Young Israel Academy of Science and Humanities and the Israel Committee for Higher Education. She is the Editor in Chief of Foundations and Trends in Signal Processing, a member of the IEEE Sensor Array and Multichannel Technical Committee and serves on several other IEEE committees. In the past, she was a Signal Processing Society Distinguished Lecturer, member of the IEEE Signal Processing Theory and Methods and Bio Imaging Signal Processing technical committees, and served as an Associate Editor of the IEEE TRANSACTIONS ON SIGNAL PROCESSING, the *EURASIP Journal of Signal Processing*, the *SIAM Journal on Matrix Analysis and Applications*, and the *SIAM Journal on Imaging Sciences*. She was Co-Chair and Technical Co-Chair of several international conferences and workshops.